Published in final edited form as:
Neuroimage. 2007 May 1; 35(4): 1401–1408.

IN VIVO AXONAL TRANSPORT RATES DECREASE IN A MOUSE MODEL OF ALZHEIMER'S DISEASE

Karen Dell Brown Smith[1], **Verena Kallhoff**[2], **Hui Zheng**[2,3,5,6], and **Robia G. Pautler**[1,4,5,**]

1*Dept. Molecular Physiology and Biophysics, One Baylor Plaza, Houston, TX 77030*

2*Dept. Molecular and Human Genetics, One Baylor Plaza, Houston, TX 77030*

3*Huffington Center on Aging, One Baylor Plaza, Houston, TX 77030*

4*Dept. Radiology, One Baylor Plaza, Houston, TX 77030*

5*Dept. Neuroscience, One Baylor Plaza, Houston, TX 77030*

6*Dept. Molecular and Cellular Biology Baylor College of Medicine, One Baylor Plaza, Houston, TX 77030*

Abstract

Axonopathy is a pronounced attribute of many neurodegenerative diseases. In Alzheimer's Disease (AD), axonal swellings and degeneration are prevalent and may contribute to the symptoms of AD senile dementia. Current limitations in identifying the contribution of axonal damage to AD include the inability to detect when this damage occurs in relation to other identifiers of AD because of the invasiveness of existing methods. To overcome this, we further developed the MRI methodology Manganese Enhanced MRI (MEMRI) to assess *in vivo* axonal transport rates. Prior to amyloid-beta (Aβ) deposition, the axonal transport rates in the Tg2576 mouse model of AD were normal. As Aβlevels increased and before plaque formation, we observed a significant decrease in axonal transport rates of the Tg2576 mice compared to controls. After plaque formation, the decline in the transport rate in the Tg2576 mice became even more pronounced. These data indicate that *in vivo* axonal transport rates decrease prior to plaque formation in the Tg2576 mouse model of AD.

Introduction

Alzheimer's disease (AD) is an age-related, neurodegenerative disease that is among the leading causes of dementia, afflicting 1% of people under the age of 60 to more than 40% of people over the age of 85 (Lindeboom and Weinstein 2004). Typical symptoms of AD are memory loss and a progressive decline of cognitive abilities (Lindeboom and Weinstein 2004). The pathological characteristics of AD are the presence of intracellular neurofibrillary tangles (NFTs) and the extracellular deposition of amyloid-beta (Aβ) aggregates, known as plaques (Gotz, Schild et al. 2004). NFTs are comprised of abnormally hyperphosphorylated tau protein, a microtubule-associated protein found primarily in axons that can block the axon when aggregated. Aβ plaques result from the sequential cleavage of the amyloid precursor protein (APP). In familial AD, mutations in APP can result in an increased amount of Aβ production leading to aggregation and formation of plaques.

** To whom correspondence should be addressed. Robia G. Pautler, Ph.D., One Baylor Plaza, BCM: 335, Houston, TX 77030, e-mail: rpautler@bcm.tmc.edu, phone: 713–798–3892

Another attribute of neurodegenerative diseases includes a progressive neuronal deterioration resulting in abnormal neuronal structure and functioning, which ultimately leads to the death of the neuron. A common feature of many neurodegenerative diseases is a progressive perturbation in normal axonal transport rates (Jablonka, Wiese et al. 2004). *In vitro* data indicates that axonal transport deficits also occur in animal models of AD. For example, in different animal models of AD, the excessive accumulation of proteins such as the tau and Aβ appear to cause a slowing of fast axonal transport, and synaptic and neuronal loss as observed in cultured rodent neurons as well as in Drosophila (Buxbaum, Thinakaran et al. 1998;Morfini, Pigino et al. 2002).

Recently, it was shown that the addition of glutamate or Aβ in cultured rat hippocampal neurons, rapidly inhibited fast axonal transport (Hiruma, Katakura et al. 2003). It was proposed that the glutamate mechanism was through activation of NMDA and AMPA receptors and Ca^{2+} influx whereas the addition of Aβ was through actin polymerization and aggregation (Hiruma, Katakura et al. 2003). Alternatively, it is thought that abnormal phosphorylation of the microtubule associated protein, tau, could be responsible for alterations in axonal transport (Morfini, Pigino et al. 2002). Increased axonopathy also occurs in animals with normal tau and double transgenic mutations in APP and Presenillin1—a genetic indicator of increased risk of AD (Suh and Checler 2002;Wirths, Weis et al. 2006). Many of the transgenic AD mouse models also exhibit axonal swelling that likely interferes with normal axonal transport (Stokin, Lillo et al. 2005;Wirths, Weis et al. 2006). A recent study also indicates that axonal swellings occur early in the Tg2576 AD model (Stokin, Lillo et al. 2005;Wirths, Weis et al. 2006). However from these combined data, it is not clear if hyper-phosphorylation of tau or neurofibrillary tangle accumulations are causal or consequential of alterations in axonal transport rates (Morfini, Pigino et al. 2002). Currently, there are not any methods available to measure *in vivo* axonal transport.

The Tg2576 mouse model of AD overexpresses a mutated form of Amyloid Precursor Protein (APP) $APP_{K670N,M671L}$ under the control of the hamster prion protein promoter and exhibit accumulation of Aβ and eventual plaque formation as aging ensues (Hsiao, Chapman et al. 1996). At the age of 6–7 months, Tg2576 mice begin to accumulate insoluble forms of Aβ 42 and Aβ 40, which aggregate to form detectable plaques starting at the age of 10 months (Kawarabayashi, Younkin et al. 2001;King and Arendash 2002;Otth, Concha et al. 2002;Puig, Gomez-Isla et al. 2004). In this study, we focus on the role Aβ has on *in vivo* axonal transport rates using the Tg2576 mouse model of AD.

We utilized the magnetic resonance imaging (MRI) contrast agent manganese ion (Mn^{2+}) in conjunction with a dynamic T_1-weighted MRI sequences to assess the transport rates of Mn^{2+} ion. Mn^{2+} has been used as a contrast agent in MRI as Mn^{2+} is a calcium analogue and is also paramagnetic (Mendonca-Dias, Gaggelli et al. 1983;Burnett, Goldstein et al. 1984;Geraldes, Sherry et al. 1986;Cory, Schwartzentruber et al. 1987;Fornasiero, Bellen et al. 1987). In MRI, Mn2+ enhancement has been effective for trans-synaptic neuronal tract tracing enabling the *in vivo* mapping of neuronal tracts (Pautler, Silva et al. 1998;Pautler and Koretsky 2002;Saleem et al. 2002;Pautler, Mongeau et al. 2003;Chuang and Koretsky 2006).

In this study, we verified the use of Manganese Enhanced Magnetic Resonance Imaging (MEMRI) from simple anatomical tract tracings to dynamic tracings reflective of axonal transport. We utilize this novel technological development to assess *in vivo* axonal transport rates in Tg2576 mice before Aβ levels increase, during Aβ accumulation and after plaque formation. By focusing on the olfactory system of the mouse we are able to access a well-defined white matter projection with minimal invasiveness to the animal. Additionally, it has been documented that the olfactory system is targeted early in the time-course of AD making

it an ideal target for monitoring disease progression (Attems, Lintner et al. 2005;Jellinger and Attems 2005).

Mn^{2+} is transported along microtubules via fast axonal transport making it possible to utilize MEMRI to dynamically measure the rates of Mn^{2+} transport, which is reflective of fast axonal transport rates, within the same animal before and during disease progression. In this study, we extend and verify the use of MEMRI from anatomic tracings to dynamic tracings reflective of axonal transport. We utilize this novel technological development to assess *in vivo* axonal transport rates in Tg2576 mice before Aβ accumulation, during Aβ accumulation and post plaque formation.

Materials and Methods

Animals

Baseline Mn^{2+} transport, temperature, and colchicine experiments were conducted utilizing eight-week-old C57/Bl6 inbred mice obtained from Baylor College of Medicine mouse facility (30 mice). Tg2576 mice overexpressing human $SwAPP695_{(K670N/M671L)}$, the Swedish mutation, were used to compare rates of axonal transport in normal and abnormal aging animals (Hsiao, Chapman et al. 1996). Male Tg2576 mice were crossed with C57Bl6/SJL F1 females to obtain Tg2576 overexpressing mice and littermate controls. A total of 28 Tg2576 animals were used for these studies.

Mn^{2+} Administration

Animals were anesthetized with ketamine/xylazine (0.75 g/ml)/(0.5 mg/ml) in phosphate buffered saline, 0.1 ml per 10 g body weight. 10 minutes after administration of the anesthesia, a nasal lavage of 4 μl of 0.75 g/ml $MnCl_2$ dissolved in nanopure water was administered and animals were allowed to recover. One hour post lavage, animals were induced on 5% isoflurane and maintained with 2% isoflurane in 100% O_2. Animals were placed in a prone position on a custom-built head holder with adjustable nose bar and secure ear pins. The respiratory rate was monitored with a pressure pad placed under the animal. Temperature was monitored by use of a rectal probe and maintained at 37ºC using both a water blanket and an air heating system (SA Instruments, Inc). Respiratory rates and temperature were monitored using the Model 1025 Small Animal Monitoring and Gating System software (SA Instruments, Inc).

MRI

Images were acquired utilizing a 9.4T, Bruker Avance Biospec Spectrometer, 21 cm bore horizontal scanner with 35 mm volume resonator (Bruker BioSpin, Billerica, MA). The imaging parameters to acquire olfactory multi-spin/multi-echo MEMRI images were as follows: TR = 500 ms; TE = 10.2 ms; FOV = 3.0 cm; slice thickness = 1mm; matrix = 128 x 128; NEX = 2; number of cycles = 15; each cycle took approximately 2 min 8 sec to acquire using Paravision software (Bruker BioSpin, Billerica, MA). Core temperature was maintained at 37ºC during scanning.

Temperature Challenge

For the temperature experiments the animals were maintained at 37.0ºC SEM 0.1 for 40 minutes. (Experiment temperature was maintained for eight minutes prior to recording for 32 minutes for a total of 40 minutes) Next, the heating system (Small Animal Instruments) was adjusted to allow the animal to cool to 30.3ºC SEM 0.3 for 40 minutes and then the animal was returned to 37.0ºC SEM 0.1 for another 40 min (Figure 3).

Colchicine Administration

Colchicine (Sigma C9754) (1 mg/kg) & vehicle controls (0.9% saline) were administered by lavage 24 hr prior to Mn^{2+} administration. Data was acquired using Paravision software (Bruker BioSpin).

Data Analysis

The region of interest (ROI) was identified and placed on an axial slice 1 mm in front of the posterior of the olfactory bulb (OB). The ROI measured 0.23 X 0.23 mm and was vertically centered on the dorsal olfactory neuronal layer (ONL) (Paxinos and Franklin 2001). The ROI was determined by measuring the length of the olfactory bulb, locating the midpoint of this line, then extending this midpoint out to the ONL using a 90º angle. The pixel closest to the midpoint within 5% error was established as the ROI for all images (Paxinos and Franklin 2001). This method of defining the region of interest ensures that the widest point of the olfactory neuronal layer is considered in the measurement. Due to a chemical shift artifact on the left olfactory bulb the ROI was localized only to the right olfactory bulb (Sbarbati, Calderan et al. 2002). This ROI was copied for each cycle and each ROI value normalized to the unaffected muscle of the same slice. The small region of interest collected in this study is representative of a single fascicle of axons projecting into the olfactory neuronal layer (Akins and Greer 2006). Mouse olfactory bulb glomeruli, the main target of an olfactory neuron fascicle, range in size from 80–150 μm (Paxinos 1995;Monnier, Bahjaoui-Bouhaddi et al. 1999). The rationale for utilizing a smaller ROI was to focus upon the fascicle projecting onto a single glomerulus to minimize any variation introduced from fascicles projecting from other regions within the olfactory epithelium. Statistical analyses: linear regression, two-tailed t-tests, and one-way ANOVA were performed with Prism (GraphPad Software, Inc).

Immunoblotting

Brain sections were dissected from 2 and 8 month old mice and immediately frozen on dry ice. The samples were homogenized in lysis buffer (1% NP40, 9.975% glycerol, 0.15M NaCl, 0.5M Tris HCl pH7.5 and protease inhibitor (Sigma)). Protein concentrations were obtained using DC Protein Assay (BIO-RAD). 20 μg of protein were loaded per well and resolved by 10% SDS-PAGE. Protein was transferred onto a Nitrocellulose membrane (BIO-RAD). The blots were blocked with 5% milk in Tris-buffered saline with 0.1% Tween-20 and incubated with 6E10 (Signet, 1:1000) or APP-C (in house, 1:1000) primary antibody. Subsequently the blots were hybridized with goat-anti-mouse or goat-anti-rabbit HRS-conjugated secondary antibody, respectively (Vector Laboratories). Bands were visualized using ECL- Western blotting detection reagents (Amersham Biosciences).

Immunohistochemistry

Olfactory bulbs were obtained from a 7.5 month and 12 month old Tg2576 animals and a 12 month old littermate control. Mice were perfused with 4% PFA and plaques were detected using 6E10 monoclonal antibody (Signet) in conjunction with R.T.U. Vectorstain kit (Vector Laboratories).

Results

Normal Manganese Transport

Our previous work demonstrated that olfactory receptor neurons (ORNs) uptake Mn^{2+} and transport the ion to the olfactory neuronal layer (ONL) of the olfactory bulb (Pautler, Silva et al. 1998). To establish the rates of normal Mn^{2+} transport along this projection, control mice were lavaged intra-nasally with a solution of $MnCl_2$ and then imaged one hour post administration utilizing our established paradigm (Pautler, Silva et al. 1998). A series of T_1-

weighted MRI images were acquired over the course of one hour in Mn^{2+} treated and control mice. MRI signal intensities in each data set were measured in the ONL and then normalized to unaltered muscle within the same slice. The location of this slice was always 1 mm anterior from the posterior edge of the olfactory bulb.

Figure 1A shows an example of the region of interest (ROI) located within the ONL as well as an example of the unaltered muscle utilized for baseline normalization. The inset of Figure 1B displays how the ROI on the olfactory bulb was selected using the length of the olfactory bulb and then finding the pixel on the ONL at the midpoint of the olfactory bulb. This pixel is representative of one fascicle within the ONL. Additionally, we tested motion correction software applied post image acquisition (Amira) and compared these data to data acquired without the motion correction. With this comparison so little motion was measured during the scans that motion correction software was determined to be unnecessary (data not shown).

The normalized signal intensity was then plotted versus time as shown in Figure 2. A linear regression curve best fit the data (Figure 2A). We verified that the gradual increase in signal intensity was due to the administered Mn^{2+} by comparing it to the slope of the control group not exposed to Mn^{2+} (Figure 2A). From Figure 2 it is evident that the slopes of Mn^{2+} treated and control animals are significantly different and that administration of Mn^{2+} results in signal intensity enhancement overtime. Figures 2B-I provide a qualitative verification of the enhancement measured in figure 2A. The slope of this curve is reflective of the rate of axonally transported Mn^{2+} (Figure 2).

Verification of Manganese Dependence on axonal transport

After establishing the baseline rate of Mn^{2+} transport, two important regulators of axonal transport, body temperature and microtubule stability were tested to validate our hypothesis that the Mn^{2+} transport rates are reflective of axonal transport (Cosens, Thacker et al. 1976;Bamburg, Bray et al. 1986;Cancalon 1988).

To evaluate the dependence on temperature, three separate transport rates were recorded from one animal at three different temperatures in sequence while the animal was still in the magnet: 37.0ºC SEM 0.1, next 30.3ºC SEM 0.3 and then returned to 37.0ºC SEM 0.1. The MEMRI data for each temperature set was recorded and analyzed as for the previously described experiments. Each of the 15 scanning cycles lasted ~2 min for a total of approximately 32 minutes at each temperature. The difference in ΔSI/Time that occurred between normal physiologic temperature and the substantially reduced temperature was significant (Figure 3. One-way ANOVA 37.0ºC vs. 30.3ºC p-value < 0.001). Once the body temperature returned to 37.0ºC, the increase in Mn^{2+} signal intensity was restored. This result demonstrates that ΔSI/Time due to Mn^{2+} transport is temperature dependent

The dependence of Mn^{2+} transport upon microtubule integrity has previously been described (Hastie 1991;Han, Malak et al. 1998). Microtubules are the primary cytoskeletal element used in fast axonal transport and are composed of α- and β-tubulin dimers. Colchicine binds to tubulin prior to polymerization, thereby inhibiting microtubule assembly and reducing axonal transport (Hastie 1991;Han, Malak et al. 1998).

We confirmed the contribution of microtubule-based transport to our dynamic MEMRI measurement. Two groups were assessed: the first group was treated with a dose of 1 mg/kg of colchicine and the second group with saline 24 hours prior to the administration of Mn^{2+}. Our results indicate that colchicine significantly reduced the ΔSI/Time when compared to control mice treated with saline (Figure 4). It is also important to note that these results demonstrate that colchicine did not stop Mn^{2+} from accumulating within the turbinates comprised primarily of axons. This data, in conjunction with the temperature studies, confirm

that Mn^{2+} transport is dependent upon axonal transport activity and machinery as colchicine is known to bind tightly to tubulin and prevent microtubule assembly.

Tg2576 mouse model of AD

We chose to conduct our studies in the olfactory system due to the presence of early olfactory involvement observed in AD patients (Solomon 1994;Thompson, Knee et al. 1998;Attems, Lintner et al. 2005), and because of the relative ease of introducing Mn^{2+} to the olfactory receptor neurons by means of nasal lavage. Therefore, it was important to confirm that the mutant form of APP was present in the olfactory bulbs of the Tg2576 mice.

The presence of mutant APP in the olfactory bulbs of Tg2576 mice was confirmed using Western Blot analyses (Figure 5A) indicating that alterations in axonal transport due to the APP mutation should be detectable utilizing MEMRI in the olfactory bulb. The axonal transport rates in the Tg2576 and littermate wildtype mice were then assessed at ages 3–4, 7–8 and 11–14 months using the established MEMRI parameters (Figure 5B).

The youngest age group, 3–4 months, demonstrated no difference in the transport rate compared to controls (Figure 5B). However, Tg2576 mice in the 7–8 month old group demonstrated a significant difference in the transport rate compared to wildtype mice of the same age (p-value <0.05) (Figure 5B). Tg2576 animals at the third and oldest time point evaluated, 11–14 months, demonstrated an even more dramatic decrease in the transport rate compared to the wildtype group (**p-value < 0.015) (Figure 5B). It is important to note that the reported differences at 7–8 months took place during the expected increase in insoluble Aβ but prior to visible plaque formation that starts at about 10 months of age (Kawarabayashi, Younkin et al. 2001). This finding was confirmed with histology of the scanned animals that showed the olfactory bulbs of the Tg2576 animals were free of plaques at 7–8 months of age (Figure 6B). Plaques were present at 12 months of age in the Tg2576 and not present in the control animal (Figure 6).

Discussion

The role of axonal transport in neurodegenerative diseases remains poorly understood. While there are indications that axonal transport deficits contribute to neurodegeneration, *in vivo* detection has been very difficult and invasive. The technique defined by this paper extends the use of MEMRI to quantify and compare *in vivo* axonal transport in normal and transgenic mouse models. This novel methodology opens up the possibility for *in vivo*, longitudinal studies that could contribute unique information in mouse models of neurodegeneration. Signal intensity data from thirty minutes of recording in the ONL allows for extrapolation of the rate (ΔSI/Time) at which Mn^{2+} is transported from the olfactory epithelium to the ONL. The difference in signal intensity produced by Mn^{2+} is also visible through qualitative assessment, as seen in Figures 2B-E. The data confirm that the nasal lavage and data acquisition are reliable and reproducible and that without Mn^{2+} the SI does not change.

It has been noted previously that physiological temperatures (36.9ºC in mice) are important for normal axonal transport (Cosens, Thacker et al. 1976;Van der Linden, Van Meir et al. 2004). To determine the effect of temperature on Mn^{2+} transport, baseline transport rates at 37.0ºC were compared to transport rates at 30.3ºC (Figure 3). The drop in temperature corresponded with a reduction in rate of Mn^{2+} transport indicating that Mn^{2+} is transported in a temperature dependent manner. Temperature dependence was further established by finding that Mn^{2+} transport rates returned to normal when the body temperature of the animal was reestablished at 37.0ºC.

Another component known to be necessary for normal axonal transport is the microtubule network. Although the role of microtubules in Mn^{2+} transport in anatomical MEMRI data has already been demonstrated (Sloot and Gramsbergen 1994;Pautler, Silva et al. 1998), we evaluated the dependence of dynamic Mn^{2+} transport upon microtubule integrity. The microtubule disruptor colchicine was utilized because it is known to bind tightly to tubulin and prevent the polymerization of microtubules (Hastie 1991;Han, Malak et al. 1998). By preventing assembly of microtubules, the ability of motor proteins to bind and transport cargo is also prevented. Colchicine has the added benefit of having been applied through nasal lavage and intracerebral injections in previous studies (Sloot and Gramsbergen 1994;Pautler, Silva et al. 1998). Here, the dose 1 mg/kg, a dose less than one-half that of previous studies, was used. Colchicine and vehicle controls (0.9% saline) were tested and results show that the colchicine significantly and dramatically blocked the rate of Mn^{2+} transport in the ONL. Data acquired using MEMRI confirmed Mn^{2+} enhancement in the olfactory turbinates at the base of the olfactory bulb, indicating continued Mn^{2+} influx into the cells and axonal areas following colchicine treatment. We paid particular attention to this because microtubule alterations are capable of changing calcium influx into the cell. The data in figure 4A-D indicate that Mn^{2+} influx was not hampered by the colchicine. The data shown here verify that Mn^{2+} transport is dependent upon microtubule-based axonal transport and that the MEMRI measurement is a quantifiable indicator of axonal transport.

Having established that Mn^{2+} transport measured by MEMRI is reflective of axonal transport, the axonal transport rates of Tg2576 animals and wildtype littermate animals were evaluated at ages 3–4, 7–8, and 11–14 months of age utilizing MEMRI. Significant differences in axonal transport between wildtype and Tg2576 mice were apparent in the 7–8 months aged group, at which point the axonal transport rate for APP overexpressing mice was 48% less than controls. When older animals, 11–14 months, were analyzed they were found to have an even more pronounced deficit, 82% less. We verified on scanned 7–8 month old animals that their olfactory bulbs were indeed negative for amyloid plaques compared to the olfactory of 12 month old Tg2576 animals with positive amyloid plaque accumulation in the olfactory bulb.

Studies analyzing Aβ accumulation, the cleavage product of APP, in these animals demonstrate that insoluble Aβ appears at 6–9 months (Kawarabayashi, Younkin et al. 2001). The definite biochemical changes take place by the 10^{th} month leaving minimal Aβ deposition followed by diffuse plaques that are visible by 12 months (Kawarabayashi, Younkin et al. 2001). Combined with the present study, this evidence suggests that the axonal transport deficits are occurring in conjunction with the accumulation of insoluble Aβ and prior to Aβ plaque formation in this particular AD model.

The cause of the differences in axonal transport rates of the Tg2576 mouse model at different ages is unclear. One possibility could be that the calcium influx is decreased resulting in less Mn^{2+} available to be transported down the axon. However, in this mouse model the calcium influx increases with age instead of decreasing suggesting that Mn^{2+} entry into the cell is equally unimpeded as our images show (Xie 2004). It has also been reported that the cytoskeletal proteins α and β tubulin are genetically up-regulated in the Tg2576 animal (Reddy, McWeeney et al. 2004). This could result in abnormal microtubule function and further strengthens our data that axonal transport decreases abnormally compared to controls.

Magnetic resonance imaging (MRI) is one of the best imaging methodologies for studying soft tissues and monitoring biological processes as they occur *in vivo*. There are currently many attempts to identify and study AD animal models through MRI imaging. Numerous MRI studies have targeted the assessment of plaque formation with and without the use of endogenously applied contrast agents (Redwine, Kosofsky et al. 2003;Helpern, Jensen et al. 2004;Helpern, Lee et al. 2004;Jack, Garwood et al. 2004;Lee, Falangola et al. 2004;Song, Kim

et al. 2004;Rohner, Staab et al. 2005;Sun, Song et al. 2005;Sykova, Vorisek et al. 2005;Vanhoutte, Dewachter et al. 2005). For example, MRI has been used to identify individual plaques in the Tg2576/Presinilin1 double mutant, a mouse model of AD (Jack, Garwood et al. 2004). Many studies have evaluated changes in anatomy, such as the high resolution, *in vitro* MRI study on fixed brains of transgenic mice containing the PDAPP mutation. The data from this *in vitro* study showed dentate gyrus shrinkage prior to the appearance of plaques (Redwine, Kosofsky et al. 2003). Other MRI studies include the assessment of alteration in the diffusion of water in the gray and white matter of mouse models of AD. This work demonstrated alterations in the diffusion of water in the Tg2576 mouse brain after plaque formation (Sun, Song et al. 2005). With the exception of the *in vitro* studies by Redwine et al, all MRI studies to date on AD mouse models have demonstrated alterations post plaque formation. Here we extend the use Manganese Enhanced MRI (MEMRI) to assess *in vivo* axonal transport, and therefore neuronal function, in the Tg2576 AD mouse model.

The data reported here establishes that functional deficits in axons begin prior to the appearance of Aβ plaques. This is supported by an *in vitro* study that found axonal swellings starting at four months in axons from mice also carrying the Swedish AD mutation (Stokin, Lillo et al. 2005). This finding implicates that axonal swellings do not form in response to amyloid deposition, but that the swellings may instigate the accumulation of Aβ similar to that seen in acute neuronal injury.

The evidence presented here indicates that MEMRI is a very promising tool for detecting early signs of abnormal physiological deficits. Using MEMRI we were able to identify and quantify the difference in axonal transport rates *in vivo* in the Tg2576 mouse model of AD during the progression of the AD phenotype. Data from the Tg2576 mouse indicates that deficits coincide with the timing of previously reported biochemical changes, but prior to histologically visible plaques. The ability to measure axonal transport rates *in vivo* opens up many new and exciting opportunities for the characterization of disease states as well as assessing the efficacy of diagnosis and therapeutic intervention.

Acknowledgements

The authors are grateful to Faridis Serrano, Mitch Deshazer, Lingyun Hu, Yingying Sun, X. Chen and N. Aithmitti for their assistance in the preparation of this manuscript. Funding for this work was provided by NIH/NINDS grant 1R21NS051274–01 [RGP], the Dana Foundation [RGP], RO1AG20670 [HZ] and RO1NS40039 [HZ].

References

Akins MR, Greer CA. Cytoskeletal organization of the developing mouse olfactory nerve layer. J Comp Neurol 2006;494(2):358–67. [PubMed: 16320244]

Attems J, Lintner F, et al. Olfactory involvement in aging and Alzheimer's disease: an autopsy study. J Alzheimers Dis 2005;7(2):149–57. [PubMed: 15851853]discussion 173–80

Bamburg JR, Bray D, et al. Assembly of microtubules at the tip of growing axons. Nature 1986;321 (6072):788–90. [PubMed: 2872595]

Burnett KR, Goldstein EJ, et al. The oral administration of MnCl2: a potential alternative to IV injection for tissue contrast enhancement in magnetic resonance imaging. Magn Reson Imaging 1984;2(4):307–14. [PubMed: 6530933]

Buxbaum JD, Thinakaran G, et al. Alzheimer amyloid protein precursor in the rat hippocampus: transport and processing through the perforant path. J Neurosci 1998;18(23):9629–37. [PubMed: 9822724]

Cancalon PF. Axonal transport in the garfish optic nerve: comparison with the olfactory system. J Neurochem 1988;51(1):266–76. [PubMed: 2454295]

Chuang KH, Koretsky A. Improved neuronal tract tracing using manganese enhanced magnetic resonance imaging with fast T(1) mapping. Magn Reson Med 2006;55(3):604–11. [PubMed: 16470592]

Cory DA, Schwartzentruber DJ, et al. Ingested manganese chloride as a contrast agent for magnetic resonance imaging. Magn Reson Imaging 1987;5(1):65–70. [PubMed: 3586874]

Cosens B, Thacker D, et al. Temperature-dependence of rapid axonal transport in sympathetic nerves of the rabbit. J Neurobiol 1976;7(4):339–54. [PubMed: 60464]

Fornasiero D, Bellen JC, et al. Paramagnetic complexes of manganese(II), iron(III), and gadolinium(III) as contrast agents for magnetic resonance imaging. The influence of stability constants on the biodistribution of radioactive aminopolycarboxylate complexes. Invest Radiol 1987;22(4):322–7. [PubMed: 3583652]

Geraldes CF, Sherry AD, et al. Magnetic field dependence of solvent proton relaxation rates induced by Gd3+ and Mn2+ complexes of various polyaza macrocyclic ligands: implications for NMR imaging. Magn Reson Med 1986;3(2):242–50. [PubMed: 3086656]

Gotz J, Schild A, et al. Amyloid-induced neurofibrillary tangle formation in Alzheimer's disease: insight from transgenic mouse and tissue-culture models. Int J Dev Neurosci 2004;22(7):453–65. [PubMed: 15465275]

Han Y, Malak H, et al. Distances between the paclitaxel, colchicine, and exchangeable GTP binding sites on tubulin. Biochemistry 1998;37(19):6636–44. [PubMed: 9578547]

Hastie SB. Interactions of colchicine with tubulin. Pharmacol Ther 1991;51(3):377–401. [PubMed: 1792241]

Helpern JA, Jensen J, et al. Quantitative MRI assessment of Alzheimer's disease. J Mol Neurosci 2004;24 (1):45–8. [PubMed: 15314248]

Helpern JA, Lee SP, et al. MRI assessment of neuropathology in a transgenic mouse model of Alzheimer's disease. Magn Reson Med 2004;51(4):794–8. [PubMed: 15065253]

Hiruma H, Katakura T, et al. Glutamate and amyloid beta-protein rapidly inhibit fast axonal transport in cultured rat hippocampal neurons by different mechanisms. J Neurosci 2003;23(26):8967–77. [PubMed: 14523099]

Hsiao K, Chapman P, et al. Correlative memory deficits, Abeta elevation, and amyloid plaques in transgenic mice. Science 1996;274(5284):99–102. [PubMed: 8810256]

Jablonka S, Wiese S, et al. Axonal defects in mouse models of motoneuron disease. J Neurobiol 2004;58 (2):272–86. [PubMed: 14704958]

Jack CR Jr, Garwood M, et al. In vivo visualization of Alzheimer's amyloid plaques by magnetic resonance imaging in transgenic mice without a contrast agent. Magn Reson Med 2004;52(6):1263–71. [PubMed: 15562496]

Jellinger KA, Attems J. Alzheimer pathology in the olfactory bulb. Neuropathol Appl Neurobiol 2005;31 (2):203. [PubMed: 15771713]

Kawarabayashi T, Younkin LH, et al. Age-dependent changes in brain, CSF, and plasma amyloid (beta) protein in the Tg2576 transgenic mouse model of Alzheimer's disease. J Neurosci 2001;21(2):372–81. [PubMed: 11160418]

King DL, Arendash GW. Behavioral characterization of the Tg2576 transgenic model of Alzheimer's disease through 19 months. Physiol Behav 2002;75(5):627–42. [PubMed: 12020728]

Lee SP, Falangola MF, et al. Visualization of beta-amyloid plaques in a transgenic mouse model of Alzheimer's disease using MR microscopy without contrast reagents. Magn Reson Med 2004;52(3): 538–44. [PubMed: 15334572]

Lindeboom J, Weinstein H. Neuropsychology of cognitive ageing, minimal cognitive impairment, Alzheimer's disease, and vascular cognitive impairment. Eur J Pharmacol 2004;490(1–3):83–6. [PubMed: 15094075]

Mendonca-Dias MH, Gaggelli E, et al. Paramagnetic contrast agents in nuclear magnetic resonance medical imaging. Semin Nucl Med 1983;13(4):364–76. [PubMed: 6359418]

Monnier Z, Bahjaoui-Bouhaddi M, et al. Structural and immunohistological modifications in olfactory bulb of the staggerer mutant mouse. Biol Cell 1999;91(1):29–44. [PubMed: 10321020]

Morfini G, Pigino G, et al. Fast axonal transport misregulation and Alzheimer's disease. Neuromolecular Med 2002;2(2):89–99. [PubMed: 12428805]

Otth C, Concha II, et al. AbetaPP induces cdk5-dependent tau hyperphosphorylation in transgenic mice Tg2576. J Alzheimers Dis 2002;4(5):417–30. [PubMed: 12446973]

Pautler RG, Koretsky AP. Tracing odor-induced activation in the olfactory bulbs of mice using manganese-enhanced magnetic resonance imaging. Neuroimage 2002;16(2):441–8. [PubMed: 12030829]

Pautler RG, Mongeau R, et al. In vivo trans-synaptic tract tracing from the murine striatum and amygdala utilizing manganese enhanced MRI (MEMRI). Magn Reson Med 2003;50(1):33–9. [PubMed: 12815676]

Pautler RG, Silva AC, et al. In vivo neuronal tract tracing using manganese-enhanced magnetic resonance imaging. Magn Reson Med 1998;40(5):740–8. [PubMed: 9797158]

Paxinos, G. The rat nervous system. San Diego: Academic Press; 1995.

Paxinos, G.; Franklin, KBJ. The mouse brain in stereotaxic coordinates. San Diego, Calif: London, Academic; 2001.

Puig B, Gomez-Isla T, et al. Expression of stress-activated kinases c-Jun N-terminal kinase (SAPK/JNK-P) and p38 kinase (p38-P), and tau hyperphosphorylation in neurites surrounding betaA plaques in APP Tg2576 mice. Neuropathol Appl Neurobiol 2004;30(5):491–502. [PubMed: 15488025]

Reddy PH, McWeeney S, et al. Gene expression profiles of transcripts in amyloid precursor protein transgenic mice: up-regulation of mitochondrial metabolism and apoptotic genes is an early cellular change in Alzheimer's disease. Hum Mol Genet 2004;13(12):1225–40. [PubMed: 15115763]

Redwine JM, Kosofsky B, et al. Dentate gyrus volume is reduced before onset of plaque formation in PDAPP mice: a magnetic resonance microscopy and stereologic analysis. Proc Natl Acad Sci U S A 2003;100(3):1381–6. [PubMed: 12552120]

Rohner TC, Staab D, et al. MALDI mass spectrometric imaging of biological tissue sections. Mech Ageing Dev 2005;126(1):177–85. [PubMed: 15610777]

Saleem KS, Pauls JM, et al. Magnetic resonance imaging of neuronal connections in the macaque monkey. Neuron 2002;34(5):685–700. [PubMed: 12062017]

Sbarbati A, Calderan L, et al. Magnetic resonance imaging of the rat Harderian gland. J Anat 2002;201 (3):231–8. [PubMed: 12363274]

Sloot WN, Gramsbergen JB. Axonal transport of manganese and its relevance to selective neurotoxicity in the rat basal ganglia. Brain Res 1994;657(1–2):124–32. [PubMed: 7820609]

Solomon GS. Anosmia in Alzheimer disease. Percept Mot Skills 1994;79(3 Pt 1):1249–50. [PubMed: 7899008]

Song SK, Kim JH, et al. Diffusion tensor imaging detects age-dependent white matter changes in a transgenic mouse model with amyloid deposition. Neurobiol Dis 2004;15(3):640–7. [PubMed: 15056472]

Stokin GB, Lillo C, et al. Axonopathy and transport deficits early in the pathogenesis of Alzheimer's disease. Science 2005;307(5713):1282–8. [PubMed: 15731448]

Suh YH, Checler F. Amyloid precursor protein, presenilins, and alpha-synuclein: molecular pathogenesis and pharmacological applications in Alzheimer's disease. Pharmacol Rev 2002;54(3):469–525. [PubMed: 12223532]

Sun SW, Song SK, et al. Detection of age-dependent brain injury in a mouse model of brain amyloidosis associated with Alzheimer's disease using magnetic resonance diffusion tensor imaging. Exp Neurol 2005;191(1):77–85. [PubMed: 15589514]

Sykova E, Vorisek I, et al. Changes in extracellular space size and geometry in APP23 transgenic mice: a model of Alzheimer's disease. Proc Natl Acad Sci U S A 2005;102(2):479–84. [PubMed: 15630088]

Thompson MD, Knee K, et al. Olfaction in persons with Alzheimer's disease. Neuropsychol Rev 1998;8 (1):11–23. [PubMed: 9585920]

Van der Linden A, Van Meir V, et al. Applications of manganese-enhanced magnetic resonance imaging (MEMRI) to image brain plasticity in song birds. NMR Biomed 2004;17(8):602–12. [PubMed: 15761949]

Vanhoutte G, Dewachter I, et al. Noninvasive in vivo MRI detection of neuritic plaques associated with iron in APP[V717I] transgenic mice, a model for Alzheimer's disease. Magn Reson Med 2005;53 (3):607–13. [PubMed: 15723413]

Wirths O, Weis J, et al. Axonopathy in an APP/PS1 transgenic mouse model of Alzheimer's disease. Acta Neuropathol (Berl) 2006;111(4):312–9. [PubMed: 16520967]

Xie CW. Calcium-regulated signaling pathways: role in amyloid beta-induced synaptic dysfunction. Neuromolecular Med 2004;6(1):53–64. [PubMed: 15781976]

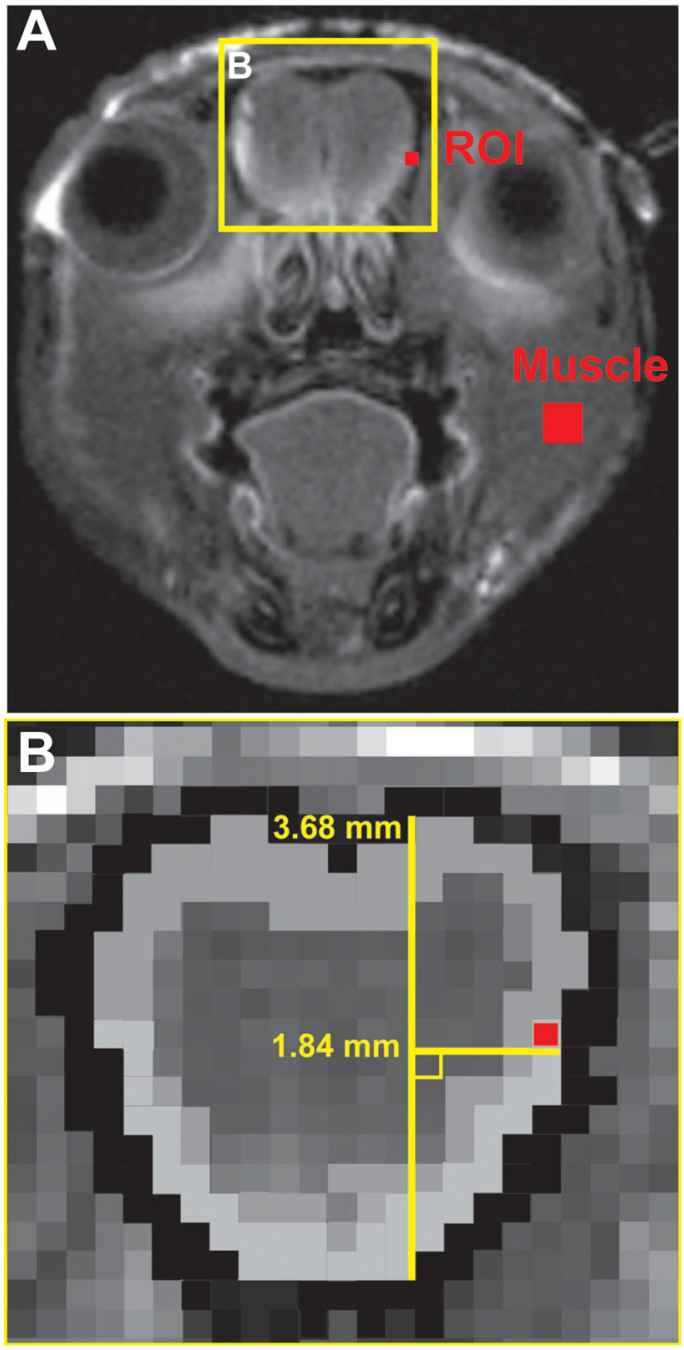

Figure 1.

A) Successive visualization of the region of interest (ROI) tracks changes in Mn^{2+} enhanced signal intensity during the second hour post Mn^{2+} lavage. Muscle used to control for background effects. B) This figure demonstrates how the ROI was determined using the length of the olfactory bulb and 90º angle to find the midpoint on the olfactory neuronal layer. Each pixel measures .23 mm.

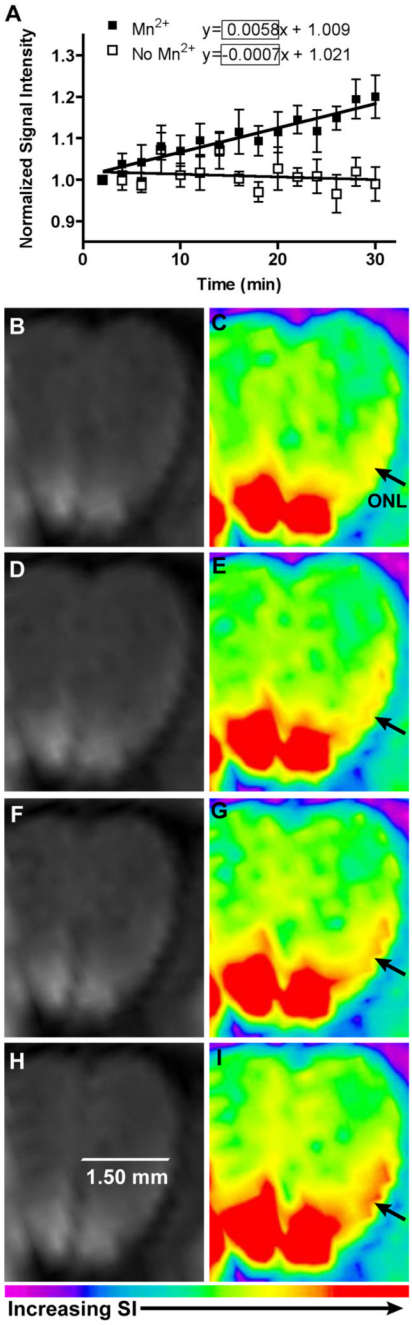

Figure 2.

A) The differences between Mn^{2+} treated and control mice (no Mn^{2+}) clearly demonstrates the increased signal intensity acquired using MEMRI. Data was quantified as a function of the change in signal intensity (ΔSI) over time (min). Slope of line acquired through linear regression. T-test of Mn^{2+} vs. no Mn^{2+} p*-value < 0.0001. * p-value is significant. (Mn^{2+} 0.00587 ± 0.001 ΔSI/time (min); n = 8; No Mn^{2+}: −0.00071± 0.001 ΔSI/time (min); n = 5.) B-I) Demonstration of movement of Mn^{2+} (red) through the olfactory bulb using sequential scans. B, C) 2 min, D, E) 12 min, F, G) 22 min, H, I) 32 min. Arrow denotes region of interest located by finding the lengthwise midpoint of the olfactory bulb and extending that point out to the ONL.

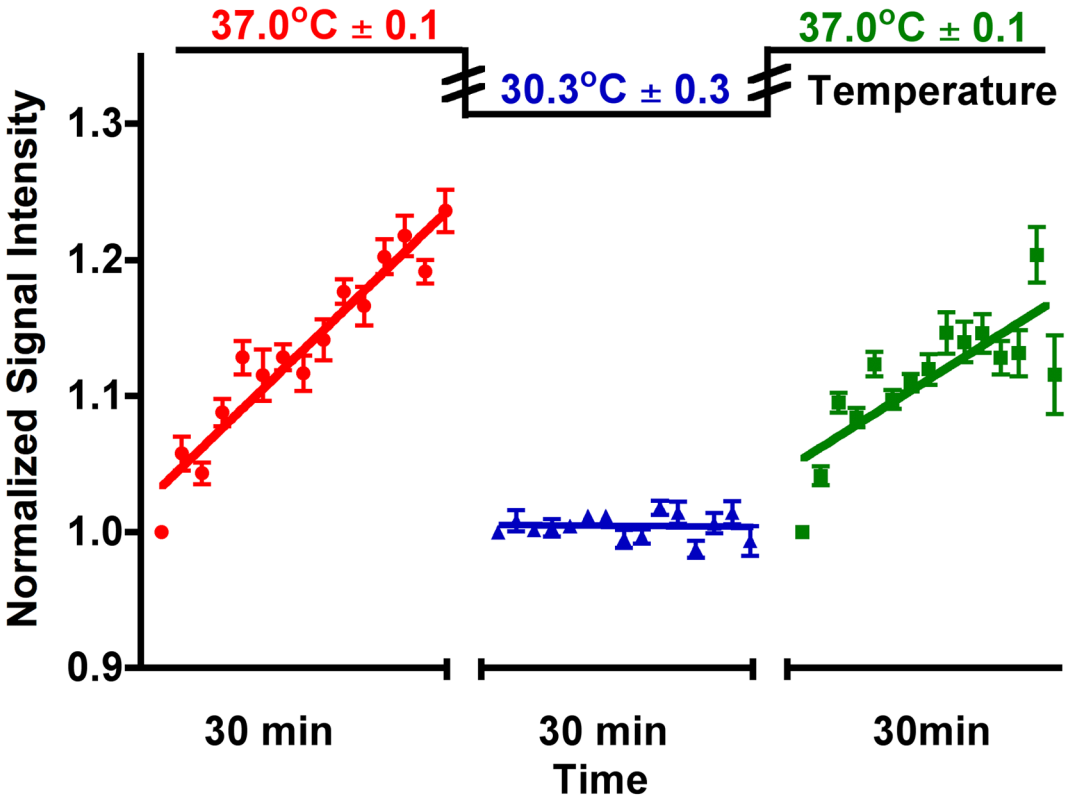

Figure 3.

Axonal transport is dependent upon body temperature. At 37.0ºC the SI increase in Mn^{2+} transport is ● 0.00679 ± 0.001, n=10 verses reduced temperature, 30.3ºC, ▲ −0.00131 ± 0.002, n=10. It also shows that the transport rate recovers with return to normal temperature (■ 0.00589 ± 0.002, n=10). Difference in ΔSI/Time (min) between both 37ºC groups and the 30.4ºC group is significant (*) with a p-value of < 0.01, df 29 (one-way ANOVA).

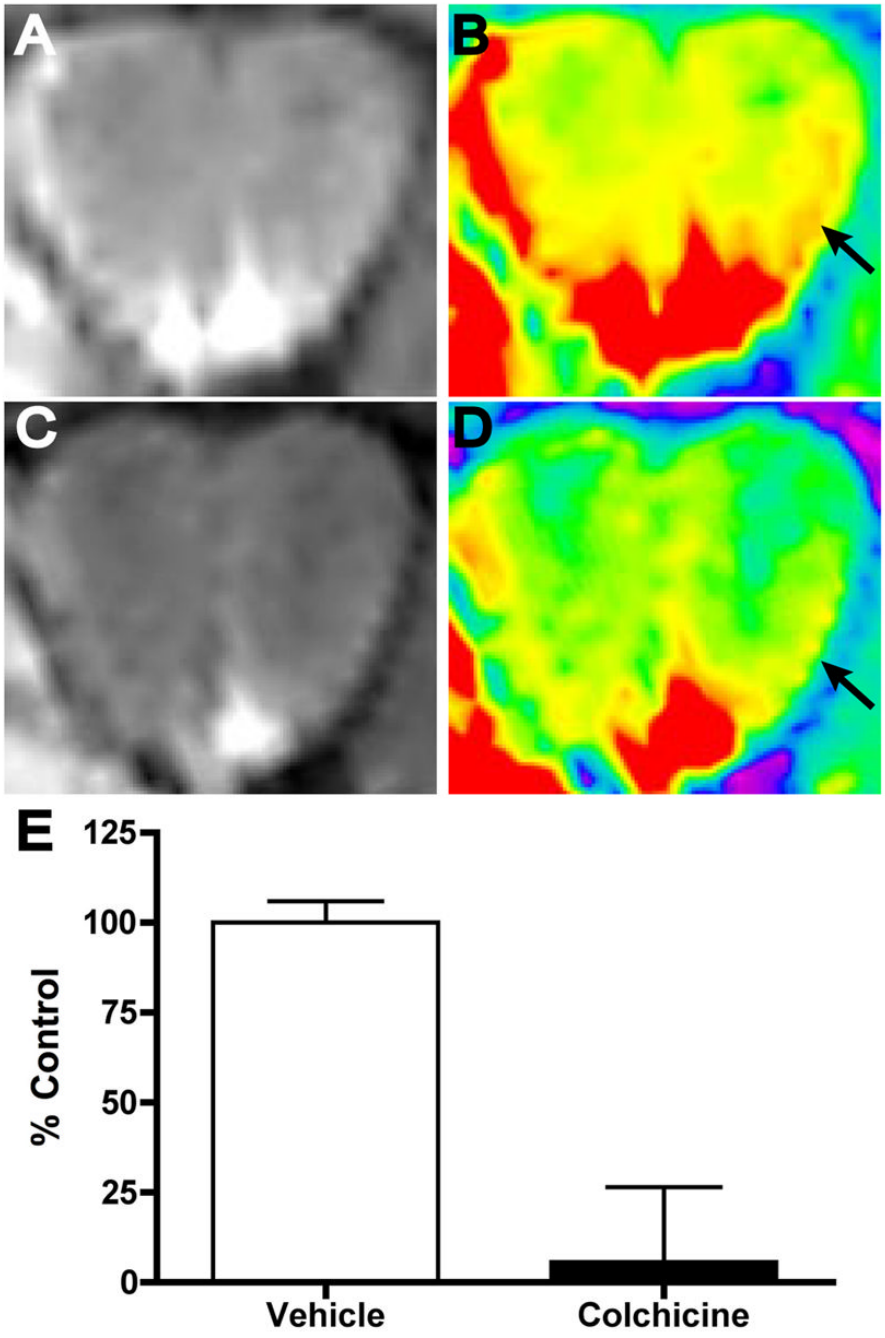

Figure 4.

A and B show the normal movement of Mn^{2+} administered 24hrs after saline lavage. C,D show Mn^{2+} reaching the base of the olfactory bulb but not traveling further, 24hrs after colchicine administration. E shows the change of normalized signal intensity of colchicine treated animals versus saline control 24 hrs after treatment. Colchicine appears to have blocked all detectable levels of Mn^{2+} transport in the ONL (labeled with arrows). (ΔSI/Time (min): vehicle=0.00101 ± 0.001 N=3; colchicine= 0.00057 ± 0.002 N=4. T-test*p-value<0.015)

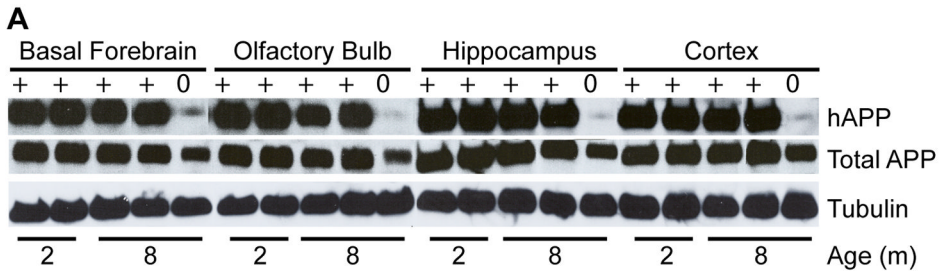

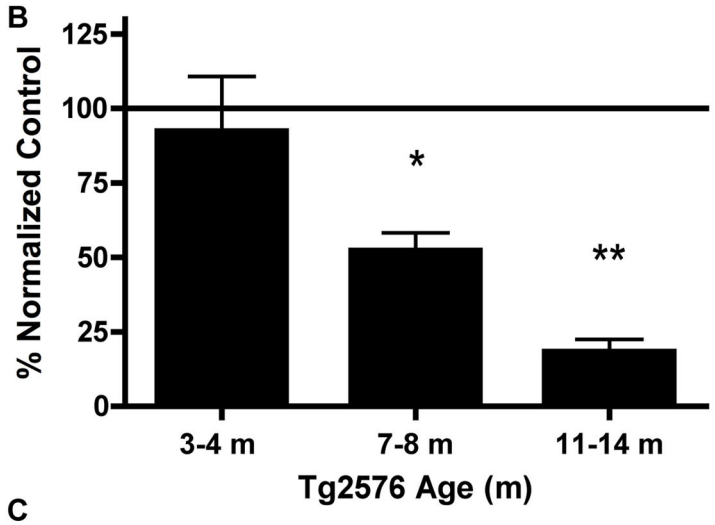

C

WT	ΔSI/Time (min)	Tg2576	ΔSI/Time (min)	t-test
3-4 m	0.00797 ± 0.0019 N=4	3-4 m	0.00737 ± 0.0015 N=4	p>0.05
7-8 m	0.00676 ± 0.0013 N=6	7-8 m	0.00353 ± 0.0004 N=6	p<0.05 *
11-14 m	0.00975 ± 0.0023 N=4	11-14 m	0.00178 ± 0.0004 N=4	p<0.015 **

Figure 5.

5A Immunoblot confirms increased human APP from the inserted transgene compared to control in different areas of the brain, specifically the olfactory bulb (Tg2576 animal = +; Control animal = 0). Figure 5B shows the gradual and significant decrease with age in the axonal transport rate of the Tg2576 mutant as percent of control (*t-test p-value<0.05 and **t-test p-value<0.015). C is the raw data for WT controls and the Tg2576 animals at the three different ages.

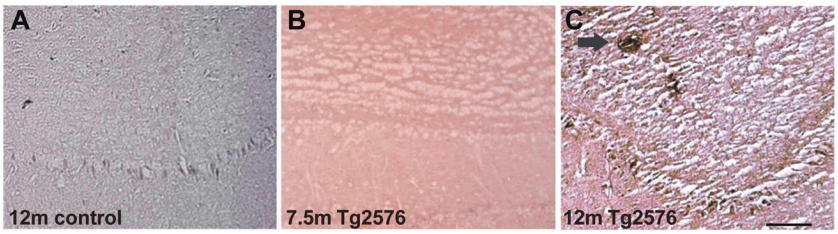

Figure 6.

A is the stained image from the control animal. B & C are the stained images of the olfactory bulbs of 7.5 & 12 month old Tg2576 animals respectively. C)The arrow points to the amyloid plaque visible at 12 months. This figure confirms that animals imaged between 7–8 months did not have plaques in the olfactory bulb when the decrease in fast axonal transport was measured and that the olfactory bulb is affected by amyloid plaque formation. m=month; scale bar = 100 μm